

Upstream Flow near Channel Exit for Free Surface Jet

Md. Yahia Hussain, Roger E. Khayat

Department of Mechanical and Materials Engineering, University of Western Ontario,

N6A 5B9, Ontario, London, Canada

rkhayat@uwo.ca

Abstract-The upstream flow near the exit of a channel for steady-state moderately inertial jet emerging from the channel is examined theoretically in this study. Poiseuille flow conditions are assumed to prevail far upstream from the exit. The problem is reduced to an eigenvalue problem governing the departure from Poiseuille flow. This is shown to be on the order of the inverse Reynolds number. The study complements Tillett's asymptotic analysis on free surface jet flow, focusing on the flow upstream from the channel exit particularly the region near the wall. Numerical calculations based on FLUENT are used for comparison, which illustrate the difficulty of conventional numerical methodologies to accurately capture the flow near the singularity, and the need for the current local asymptotic analysis.

Keywords-Free-surface Jet; Moderate Reynolds Number; Exit Singularity; Upstream Flow; Asymptotic Matching

I. INTRODUCTION

Liquid laminar jets have been extensively studied previously in the literature. However, the focus has mainly been on the jet flow downstream from exit. In addition, in most studies of Newtonian jets, due to the convective nonlinearities, limited studies can be found which take inertial effect into account. For high inertial jet flow, Tillett [1] used the method of matched asymptotic expansions for a planar steady free surface jet as displayed schematically in Fig. 1. The figure depicts the entire jet domain (Fig. 1a) and the domain of computation using dimensionless notations (Fig. 1b).

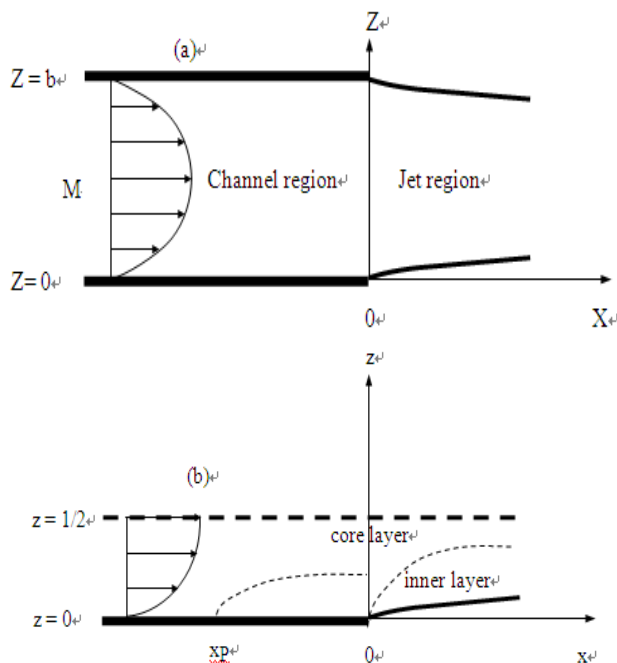


Fig. 1 Schematic illustration of the flow configuration: (a) the channel and jet regions are shown, using dimensional notations; (b) computation domain including the boundary layer heights using dimensionless notations

When the fluid exits the channel, the vanishing of the wall shear stress causes a boundary layer to develop adjacent to the wall and free surface, the inner layer. The flow in this thin layer and the jet contraction affect the core of the jet. Unlike the inner layer, this core layer extends over both the upstream and downstream regions. In each layer, different physical mechanisms dominate the flow, with corresponding characteristic length scales. In particular, the boundary and inner layers are shear dominated and the flow is of the boundary layer type. In the core layer, both shear and elongation are in balance as a result of the predominance of the Poiseuille character of the flow and the influence of the contracting jet. Nevertheless, the core layer remains predominantly of inviscid rotational nature given its relative remoteness from the free surface and the channel walls.

Tillett developed a classical matched asymptotic analysis to find the flow at small distances downstream of the jet. In this case, a boundary layer flow is sought in the inner layer near the free surface, which is matched to the core solution. Similarly to all boundary layer analyses, where the solution is not valid within a small distance from inception such as very near the leading edge and stagnation point, Tillett's analysis precludes the flow at the channel exit. However, the distance in question is small, on the order of the (local) boundary layer thickness. Consequently, the boundary layer approach turns out to be successful in capturing the flow nature near inception and jet profile. Miyake et al. [2] carried out a similar analysis to Tillett's on a vertical jet of inviscid fluid taking gravity into account. Philippe and Dumargue [3] also applied a similar analysis to Tillett's for viscous axisymmetric vertical jets, emphasizing the interplay between gravity and inertia, and their influences on the free surface shape and the velocity profile. Poiseuille conditions were assumed at the duct exit. A local similarity transformation was carried out by Wilson [4] for the axisymmetric viscous-gravity jet for the boundary-layer type flow close to the free surface. More recently, Saffari and Khayat [5] extended Tillett's analysis to include viscoelastic effects. For a recent perspective on asymptotic analyses, their applications and historic development, the reader is referred to the book by Sobey [6] on interactive boundary layer and triple-deck theory. In this regard, a triple-deck approach is not exactly applicable for the current problem given the absence of an inviscid (external) layer. A treatment of closer relevance to the current problem would be that of Smith [7-9] on the flow in a tube with (axisymmetric) constriction. Smith realized that a similar model to the triple-deck formulation, based on an inviscid rotational core flow region together with viscous boundary layer type region near the wall, could be applied to the flow in the vicinity of the constriction. In particular, in contrast to the flow over a mild constriction, there is upstream influence for the flow over a severe constriction [9] (more discussion will follow shortly).

The current paper examines closely the flow near the wall inside the channel, and the entire upstream flow region from the channel exit, which was not analyzed by Tillet [1]. In fact, the upstream flow solution near the wall was not required in Tillet's analysis. Only the flow in the core region (far from the wall) was required in order to determine the flow and the free surface shape of the jet outside the channel. Recall that Tillet's analysis requires the matching of the flow between the inner and core layers outside the channel, and the matching of the core flow outside the channel to the core flow inside the channel. Therefore, Tillet did not need to match the inner flow near the jet free surface since a similarity solution was sought with the flow near the wall upstream from the channel exit. Consequently, Tillet did not obtain the entire flow upstream from the exit.

In the present study, the interplay between inertia and viscous effects upstream from the channel exit is investigated for moderately inertial jet flow. The formulation and solution procedure follow those of the channel entry flow [10-12]. In order to match the solution with Tillet's core solution outside the channel, the flow field inside the channel is taken as superposition of the Poiseuille flow and the deviation from it, similarly to the approach adopted for entry flow. For further validation of the current formulation, and to highlight the difficulty associated with fully computational methodologies, the predicted flow field is compared with the one based on the computational fluid dynamics software Fluent. Finally, the present approach can be generalized to tackle other laminar high-Reynolds number flow processes of important practical interest near channel or pipe exits, such as wall jet or coating flows [13], extrusion and related processes [14], fiber spinning [15] and film casting [16].

II. GOVERNING EQUATIONS AND BOUNDARY CONDITIONS

The fluid examined in this study is assumed to be incompressible of density ρ and kinematic viscosity ν . The flow of the jet emerging from the channel is schematically depicted in Fig.1 in the (X, Z) plane. The X-axis is taken along the lower edge of the channel and the Z axis is chosen in the transverse direction across the exit (X = 0). It is assumed that near the exit inside the channel, the boundary layer starts to develop at X = X_p at which point deviation from Poiseuille behavior begins. Following Tillet [1], non-dimensional variables are introduced by measuring lengths with respect to the channel width, b, stream function with respect to Ab², where Ab is the mean velocity, and pressure with respect to $\rho A^2 b^2$. The Reynolds number is given in this case as Re = Ab²/ ν . The inverse Reynolds number will be the small parameter in the problem. Accordingly, the non-dimensional conservation of momentum equations for the laminar steady flow take the following form

$$\Psi_z \Psi_{xz} - \Psi_x \Psi_{zz} = -p_x + \text{Re}^{-1} (\Psi_{xxz} + \Psi_{zzz}) , \quad (2.1a)$$

$$-\Psi_z \Psi_{xx} + \Psi_x \Psi_{xz} = -p_z - \text{Re}^{-1} (\Psi_{xxx} + \Psi_{zzz}) . \quad (2.1b)$$

Given the flow symmetry, the problem is examined over the range $0 \leq z \leq \frac{1}{2}$; the flow for $\frac{1}{2} \leq z \leq 1$ can be obtained similarly. Inside the channel, the following conditions must be satisfied, namely, the conditions of symmetry, adherence and no penetration at the wall, the far upstream fully developed flow, and the matching with Tillet's profile at the exit that read respectively:

$$\Psi_z (x, z = 0) = \Psi_x (x, z = 0) = 0 , \quad (2.2b)$$

$$\Psi (x \rightarrow -\infty, z) = \Psi_0(z) , \quad (2.2c)$$

$$\Psi (x = 0, z) = \Psi_T (x = 0, z) , \quad (2.2d)$$

where $\Psi_0(z) = z^2 - \frac{2}{3}z^3$ is the stream function for Poiseuille flow, and

$$\Psi_T (x \leq 0, z) = \Psi_0(z) + \text{Re}^{-1} \sum_{n=1}^{\infty} \frac{A_n}{\beta_n} e^{\beta_n x} V_n(z) , \quad (2.3e)$$

is the stream function from Tillet's solution, written here in terms of the inverse Reynolds number. Note that Tillet's solution is valid in the core region far from the wall. Here A_n and β_n are constants, and V_n are orthogonal functions of z [1]. Incidentally, these constants have been recalculated and found to be in disagreement with Tillet's values. For this reason, the corrected (current) values are reported in Table I for reference.

TABLE I VALUES OF A_n AND β_n FOR THE FIRST EIGHT MODES

n	β_n	A _n
1	5.179	8.11
2	11.941	5.37
3	18.396	4.82
4	24.772	4.58
5	31.114	4.45
6	37.439	4.36
7	43.753	4.30
8	50.061	4.25

At the channel exit, x = 0, the shear stress undergoes a step change from a non-zero value at the lower wall, z = 0, to zero at the free surface, z = $\zeta(x)$. The effect of this drop diffuses upstream inside the channel (x < 0) over a distance X_p where fully developed Poiseuille flow is recovered, and downstream (x > 0) over a distance X_∞ at which point the flow is entirely of the boundary layer type. The solution for x > 0 was entirely worked out by Tillet [1], and will only be referred to when needed, for reference or completeness. The flow is supposed to have the basic Poiseuille profile (2.2c) to lowest order and is modified when the fluid leaves the channel in the form of the jet.

Following Tillet's argument [1], when the fluid detaches itself from the wall of the channel, a situation similar to the flow near the leading edge of a plate, the abrupt vanishing of the wall shear stress causes a boundary layer to form in a region near the free surface downstream as well as along the channel wall upstream (see Fig.1). The boundary layer regions reflect the deviation of the flow near the wall and free surface from the asymptotic core flow. Note that the core flow is not

exactly Poiseuille since “the parabolic velocity profile adjusts itself close to the exit so as to satisfy the condition of zero traction at the free surface.” At infinite Reynolds number, or in the inviscid limit, the stress free condition at the free surface cannot be imposed since there is no viscous mechanism for the stress singularity to diffuse. In this limit, Poiseuille flow remains unaltered as the fluid exits the channel, with the jet remaining straight; no contraction or expansion occurs. Since no uniqueness theorem exists in the inviscid limit, it is assumed that the fully developed Poiseuille flow is everywhere the solution at infinite Reynolds number [1]. “With this assumption, the flow in the core of the jet, to lowest order, is not affected by the flow in the boundary layer region” near the free surface outside the channel and near the wall inside the channel, although the boundary layer is expected to induce perturbations to the basic Poiseuille flow, when higher order terms are included, both for the flow upstream and downstream from the channel exit. This assumption is similar to the one made by Smith [9] for the tube flow with severe constriction, where the flow field in the core region, to leading order, satisfies the inviscid equations of motion.

III. PROBLEM FORMULATION AND SOLUTION PROCEDURE

As mentioned earlier, the present study focuses on the flow upstream of the channel exit, particularly near the wall. A uniformly valid flow is now obtained for $x < 0$, which is considered to be a superposition of the Poiseuille flow and the deviation from it at high Reynolds number.

A. The Departure from Poiseuille Flow

Based on condition (2.3), the corresponding stream function and pressure may be expressed as

$$\psi(x, z) = \psi_0(z) + \text{Re}^{-1} \hat{\psi}(x, z), \tag{3.1a}$$

$$p(x, z) = \text{Re}^{-1} \hat{p}(x, z), \tag{3.1b}$$

It is observed that, terms of lower order, involving Re^{-a} where $0 < a < 1$, are not required. This is a direct consequence of the need to match the current solution (3.1) with Tillett’s at the channel exit. The basic character of the flow, given here by (3.1), is similar to the laminar flow in a channel or a tube with constriction [7-9] at high Reynolds number. Particularly, for fine and mild constrictions, the fully developed (Poiseuille) profile is the flow to leading order. Smith examined the flow for fine, moderate [7, 9] and severe [9] constrictions. The severity of the constriction is reflected in the characteristic slope of the obstacle, which is of $O(\text{Re}^{-1/3})$ and $O(\text{Re}^{-1/6})$ for fine and moderate constrictions, respectively. Here Re is Smith’s Reynolds number based on the tube diameter and the maximum velocity. In these situations, there occurs virtually no nonlinear upstream influence of the obstacle, and, similarly to (3.1), the core flow is just an inviscid rotational perturbation of the basic Poiseuille flow.

In contrast, in a severe constriction, where the obstacle slope is of $O(1)$, there is significant upstream influence on the core flow. Note that the flow field expansion takes the same form regardless of the constriction level of severity. Thus, Smith’s expansion for the flow with any constriction is the same as the current expansion (3.1). In general, Smith gives the core flow as

$$\psi, u, p = (\psi_0, u_0, p_0) + \text{Re}^{-M} (\psi_1, u_1, p_1) + o(\text{Re}^{-M}),$$

where $M > 0$ and (ψ_0, u_0, p_0) satisfy the inviscid equations of motion. However, in contrast to (3.1), for a severe constriction, Smith’s leading order terms in stream function and pressure do not exactly correspond to fully developed flow, but still satisfy the inviscid equations of motion. Smith found that the viscous separation ahead of the constriction occurs in a viscous wall zone, whose thickness is $o(\text{Re}^{-1/3})$ for the balance of inertial and viscous forces.

Upon eliminating the pressure, substituting (3.1) and neglecting terms of higher order than $1/\text{Re}$, equations (2.1) lead to the following equation for the deviation in stream function, namely

$$2 \text{Re} \left[(z - z^2) (\hat{\psi}_{xxx} + \psi_{xxx}) + 2\psi_x \right] = \psi_{xxx} + 2\psi_{xxx} + \psi_{zzz} \tag{3.2}$$

The solution of (3.2) is sought in the form:

$\hat{\psi}(x, z) = \sum_{n=1}^{\infty} B_n e^{\alpha_n x} U_n(z)$, where the shape functions $U_n(z)$ and corresponding eigenvalues α_n (here assumed to be real and positive) satisfy the following problems:

$$2\alpha_n \text{Re} \left[(z - z^2) (U_n'' + \alpha_n^2 U_n) + 2U_n \right] = \alpha_n^4 U_n + 2\alpha_n^2 U_n'' + U_n^{iv} \tag{3.3a}$$

$$U_n(0) = U_n'(0) = U_n(1) = U_n'(1) = 0. \tag{3.3b}$$

The coefficients B_n will be determined by applying condition (2.3d). The solution of problem (3.3) can be sought using methodologies used for entry flow [10-12]. However, the following procedure is suggested and used in the current study, which seems to be more convenient.

B. Solution of the Eigenvalue Problem

The solution of problem (3.3) is carried out using two methods, one to conveniently seek an accurate estimate and number of the eigenvalues, and the other to determine accurately both eigenvalues and corresponding eigenfunctions. The first method consists of expanding $U_n(z)$ in terms of Chandrasekhar functions [17]. In this case, if (3.3a) is rewritten as $L(U_n, \text{Re}, \alpha_n) = 0$, where L is the corresponding linear operator, then the solution, which satisfies conditions

(3.3b), is sought in the form $U_n(z(y)) = \sum_{i=1}^{\infty} U_{ni} S_i(y)$ Here, $y \in [-1/2, 1/2]$ and $S_i(z)$ are the odd Chandrasekhar functions given by [17]

$$S_i(y) = \frac{\sinh(\mu_i y)}{\sinh(\mu_i / 2)} - \frac{\sin(\mu_i y)}{\sin(\mu_i / 2)}, \tag{3.4}$$

where the constants μ_i are the roots of $\tanh(\mu_i / 2) - \tan(\mu_i / 2) = 0$. The constant coefficients U_{ni} are determined upon carrying out a Galerkin projection of (3.3a), leading to the following system of algebraic equations:

$$\left\langle L \left(\sum_{i=1}^{\infty} U_{ni} S_i(y), \text{Re}, \alpha_n \right) S_j(y) \right\rangle = 0, \tag{3.5}$$

where the brackets denote integration over the interval $[-1/2, 1/2]$. In turn equation (3.5) yields the following relation for the eigenvalues α_n :

$$\left[2\alpha_n \operatorname{Re} \left(C_{1ij} + \alpha_n^2 C_{2ij} \right) \right] + \alpha_n \left(4 \operatorname{Re} - \alpha_n^3 \right) \delta_{ij} - 2\alpha_n^2 C_{3ij} - C_{4ij} = 0, \quad (3.6)$$

where

$$\begin{aligned} C_{1ij} &= \left\langle \left(0.25 - y^2 \right) C_i''(y) C_j(y) \right\rangle \\ C_{2ij} &= \left\langle \left(0.25 - y^2 \right) C_i'(y) C_j'(y) \right\rangle \\ C_{3ij} &= \left\langle C_i''(y) C_j(y) \right\rangle \\ C_{4ij} &= \left\langle C_i''''(y) C_j(y) \right\rangle = \lambda_i^4 \delta_{ij} \end{aligned} \quad (3.7)$$

Once the eigenvalues are determined (approximately) from (3.6), they are used as initial guess for the solution of (3.3). The solution of the two-point boundary-value problem is sought using MATLAB.

C. Eigenvalues and Convergence

The influence of the Reynolds number is illustrated for the first three eigenvalues in Fig. 2.

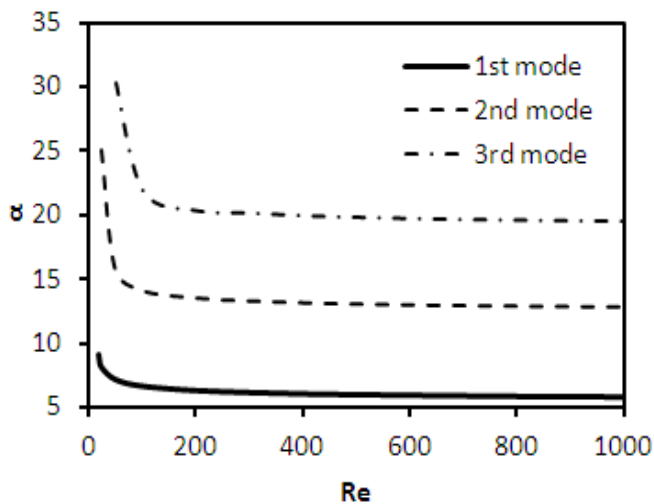


Fig. 2 Dependence of the first three eigenvalues on the Reynolds number

All eigenvalues appear to exhibit a singularity at some small Reynolds number, which is larger for the higher modes. Typically, the eigenvalue decreases rapidly in the moderately low Reynolds number range and levels off in the large Re range. The rate of decrease diminishes for the higher modes. This behaviour is reminiscent of the one encountered for entry flow [12].

The influence of the number of modes, M, is illustrated in Fig. 3, where the departures in steam function (Fig. 3a) and streamwise velocity component (Fig. 3b) are plotted against height at $x = -0.1$ for $Re = 500$. Convergence is rather rapid but not necessarily monotonic. The oscillatory convergence is depicted from the inset in Fig. 3b where $\hat{u}(x = -0.1, z = 0.5)$ is plotted against M. Convergence is essentially attained for $M > 4$. Thus, only a relatively small number of modes will be needed. Convergence is expected to be even faster the further the flow is from the exit.

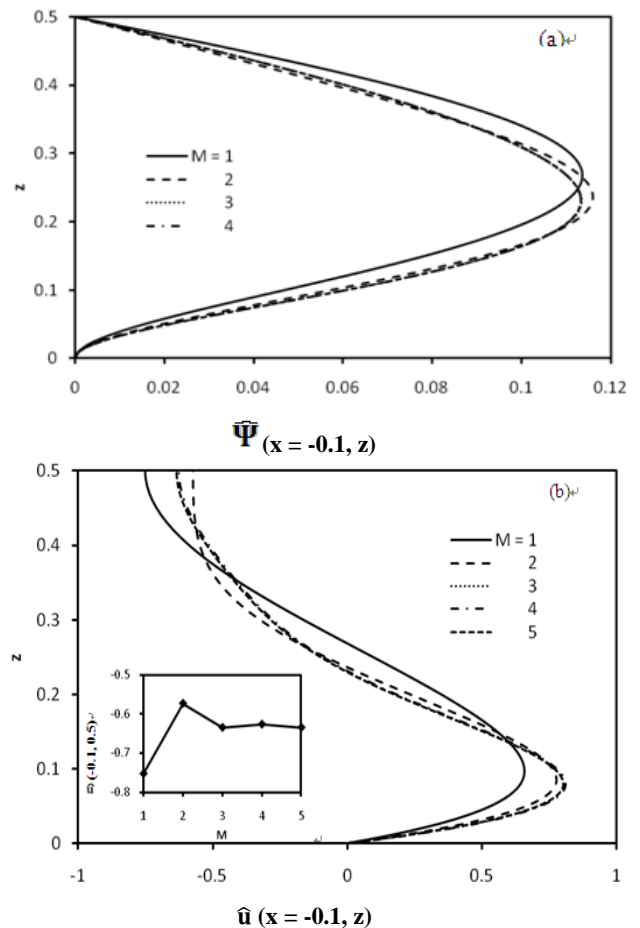


Fig. 3 Behaviour of $\hat{\psi}(x = -0.1, z)$ (a) and $\hat{u}(x = -0.1, z)$ (b) for different number of modes, M, and $Re = 500$. Inset in (b) shows $\hat{u}(x = -0.1, z = 0.5)$ vs. the number of modes

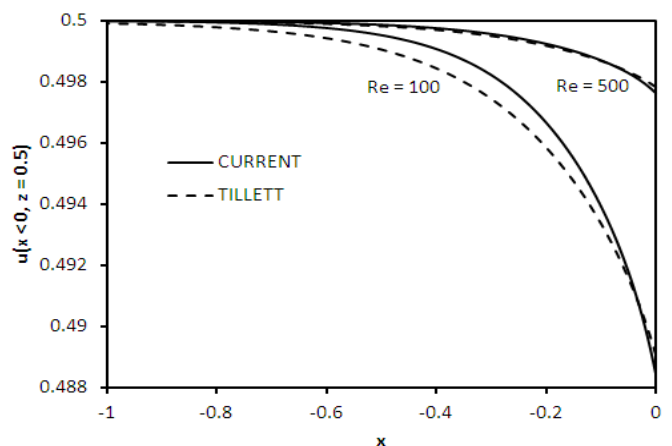


Fig. 4 Distribution of the streamwise velocity component along the centerline for $Re = 100$ and 500 based on the current (solid lines) and Tillett's (dashed lines) formulation

Further validation is carried out upon comparison with Tillett's core solution. As mentioned earlier, Tillett's solution remains valid in the core region far from the wall, and should agree with the solution based on the current formulation in the core region. Indeed, Fig. 4 illustrates this agreement between the current formulation and Tillett's solution. The figure displays the dependence of $u(x, z = 0.5)$ on x along the centerline for $Re = 100$ and $Re = 500$. Clearly, regardless of the Reynolds number, agreement is generally very close.

There is essentially no deviation between the two formulations for $Re > 300$.

IV. INFLUENCE OF INERTIA ON THE FLOW FIELD

The influence of inertia on the flow field, including the velocity, pressure, and stress is considered in this section. The boundary layer structure near the wall inside the channel and the free surface outside the channel will be examined in the next section. Fig. 5 displays the distributions of the streamwise (Fig. 5a) and depthwise (Fig. 5b) velocity components, as well as the pressure (Fig. 5c) across the channel at different positions. In this case, $Re = 100$. Note that $Rep(x, z)$ is plotted in Fig.5c. The streamwise velocity profiles in Fig.5a retain essentially their parabolic character for any position; no change in concavity is detected. Closer agreement with Poiseuille flow is of course predicted as Re increases (not shown).

Upon approaching the channel exit the flow exhibits some flattening, which nevertheless remains far from plug flow condition. There is little qualitative change along the channel. Generally, the profiles tend to intersect at a common height ($z \approx 0.2$ in this case), with the flow being slower (faster) above (below) this point. Additional insight is inferred from the departure profiles from Poiseuille flow as depicted from the inset in Fig.5a. The departure velocity exhibits a maximum below the intersection. Although the maximum strengthens with x closer to zero, the height location of the maximum appears to be independent of x . As expected, the depthwise velocity profiles exhibit a maximum of increasing strength upon deviation from the fully developed, or $w(x \rightarrow -\infty, z) = 0$, limit. The maximum strengthens near the channel exit with additional modulation, which is somewhat more apparent from the pressure profiles. These profiles in Fig. 5c display the most significant qualitative change with x . In this case, there is a change in concavity and deviation from monotonic behavior as the exit is approached. Note that the pressure at the plate ($z = 0$) is equal to the Poiseuille level, $p(x, z = 0) = -4x/Re$, which becomes itself equal to zero at the channel exit ($x = 0$). The maximum deviation from the Poiseuille limit in pressure occurs at the centerline ($z = 0.5$), which is expected given the symmetric contraction of the jet. However, the pressure profiles exhibit a local weaker minimum as the fluid approaches the channel exit, and eventually more pronounced modulation at $x = 0$.

The overall influence of inertia is assessed upon examining the flow properties along the centerline ($z = 0.5$) and the wall ($z = 0$). Fig. 6 displays the streamwise velocity component along the centerline (Fig. 6a) and the magnitude of the shear stress, $\tau_w(x)$, at the wall (Fig.6(b) for different levels of inertia. The pressure distribution along the centerline remains essentially the same as Tillet's [1] and will not be shown here. Note that Poiseuille flow corresponds to the $\lim_{x \rightarrow -\infty, z = 0.5} u = 0.5$, $\lim_{x \rightarrow -\infty} \tau_w = 2$ and $\lim_{x \rightarrow -\infty, z = 0.5} p = -4x / Re$. The deviation from Poiseuille flow grows monotonically with x to continue to increase outside the channel. In fact, the velocity decreases slightly from the Poiseuille level inside the channel, reflecting the flattening of the velocity profile reported in Fig. 5a as the exit is approached. The velocity continues to decrease faster (essentially linearly) with x outside the channel, while the pressure decays to zero (not shown). The wall shear stress

increases as the fluid approaches the exit, again as a result in velocity flattening and the adherence of the fluid to the wall. This is reminiscent of the behavior observed by Gottlieb and Bird for shear thinning fluids [18].

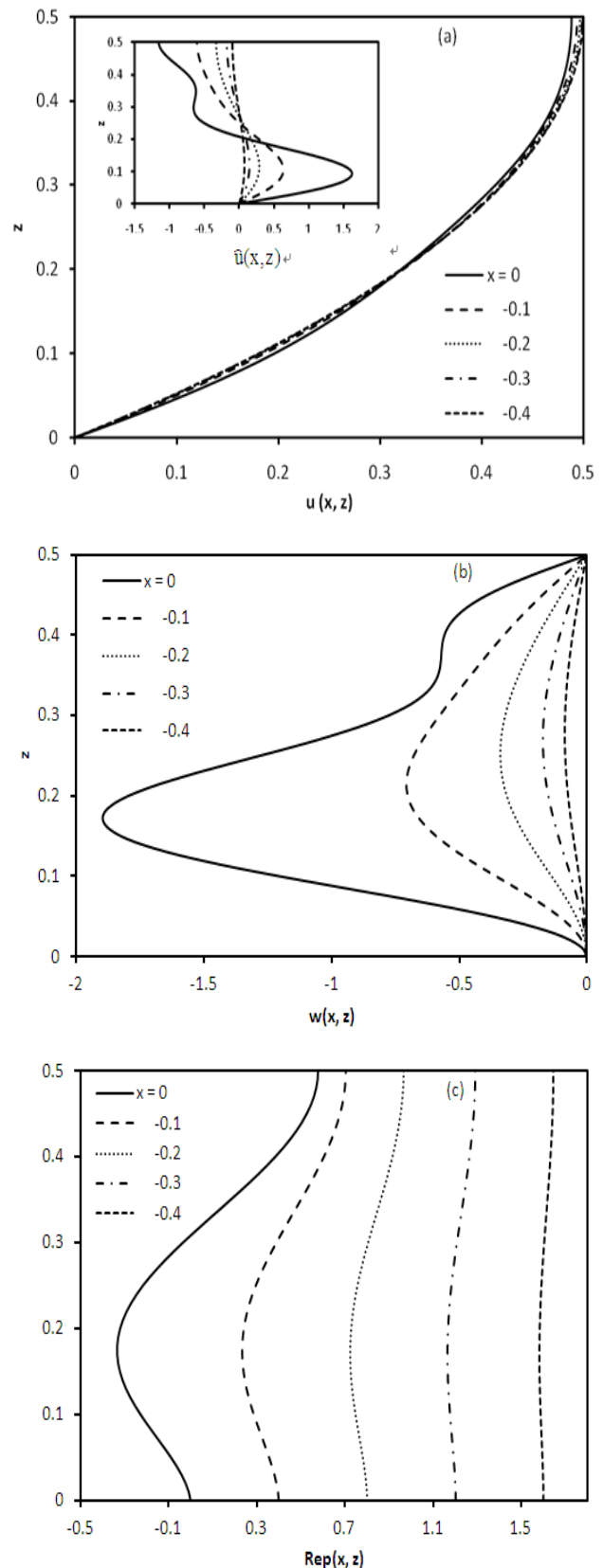


Fig. 5 Profiles of the streamwise (a), depthwise (b) velocity components, and the pressure (c) across the channel at different positions for $Re = 100$ Inset in (a) shows the profiles of the departure $\hat{u}(x, z)$ from Poiseuille flow

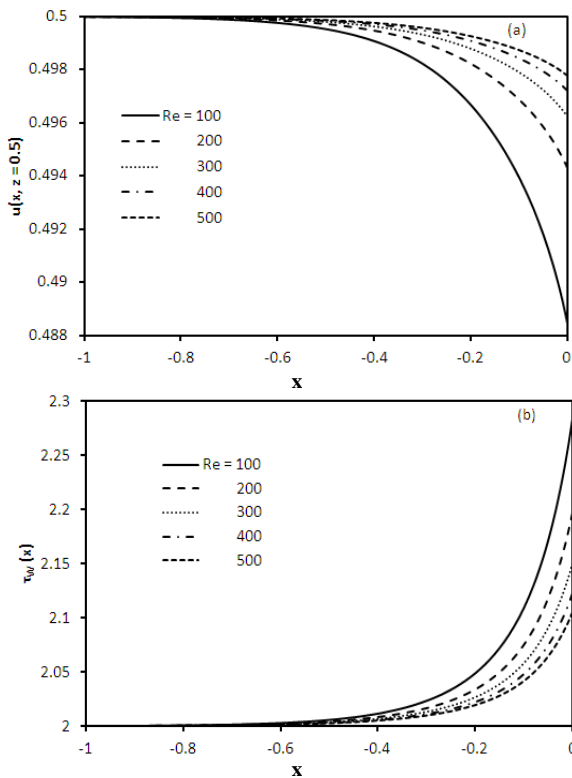


Fig. 6 Variation of (a) centerline velocity and (b) the wall shear stress with position at different Reynolds numbers

While the pressure distribution (see Tillett’s Fig. 3) suggests that Poiseuille conditions are essentially recovered for $x < -0.5$, independently of the Reynolds number, the velocity and wall shear stress distributions reflect a strong dependence on inertia of the point of recovery of fully developed flow depending on which flow variable criterion is used. Although Fig. 6a and 6b appear to suggest that both the centerline velocity and wall shear stress lead to the same position, $x = x_P$, where Poiseuille flow is practically recovered, this is not the case given the difference in scale ranges between the two figures. Fig. 7 displays the dependence of x_P on Re , which suggests, as expected, that Poiseuille conditions are recovered further upstream from the channel exit as inertia decreases. However, the position of the recovery point depends on the criterion used to determine it. Fig. 7 displays the dependence of x_P on Re based on the centerline velocity and pressure as well as the wall shear stress. The centerline velocity criterion tends to overestimate x_P while the wall shear stress criterion tends to underestimate it. The centerline pressure criterion gives a level in between.

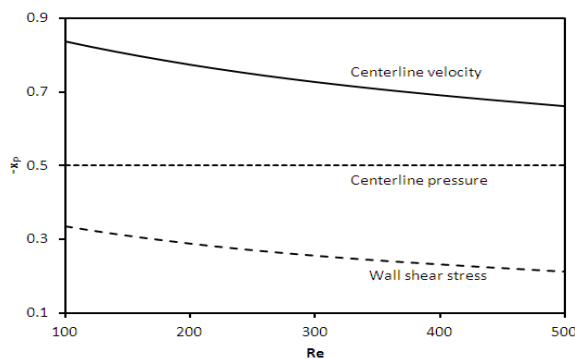


Fig. 7 Influence of inertia on the position where the flow departs from Poiseuille behaviour based on the centerline velocity, the wall shear stress and centerline pressure

V. BOUNDARY LAYER STRUCTURE

In this section, the boundary layer thickness will be examined based on dimensional arguments and calculations. Both the boundary layer near the wall inside the channel and near the free surface of the jet outside the channel will be examined. It is helpful to first estimate the boundary layer thickness, $\delta(x)$, using dimensional arguments. Suitable reference length and velocity are required in each region. Generally, the boundary layer thickness may be expressed in terms of a dimensionless transverse diffusion time, t , as

$$\delta \sim \left(\frac{1}{Re}\right)^{1/2}$$

and the velocity may be expressed in terms of the corresponding axial convection length as $u(x, z) \sim \frac{x}{t}$, where

x refers to the distance from an appropriately defined origin ($x = 0$ outside the channel and $x = x_P$ inside the channel).

Eliminating t , leads to $\delta(x) \sim \left(\frac{x}{u Re}\right)^{1/2}$. The velocity based

on the current formulation and Tillett’s core solution will be used to determine the dependence of $\delta(x)$ for $x < 0$ and $x > 0$, respectively, on the Reynolds number and position.

A. Boundary Layer Inside the Channel

For the flow inside the channel, a suitable choice for u is the velocity based on Tillett’s core solution (2.3), which yields

$$u_T(x \leq 0, z) = u_0(z) + Re^{-1} \sum_{n=1}^{\infty} \frac{A_n}{\beta_n} e^{\beta_n x} V_n'(z) \tag{5.1}$$

The reference velocity will be taken at the centerline, or

$$u_T(x, 0.5) = 0.5 + Re^{-1} \sum_{n=1}^{\infty} \frac{A_n}{\beta_n} e^{\beta_n x} V_n'(0.5)$$

This yields in turn the following estimates for the boundary layer thickness:

$$\delta(x_P < x < 0) \sim \left(\frac{x - x_P}{Re}\right)^{1/2} + O(Re^{-3/2}) \tag{5.2}$$

As expected, the boundary layer thickness grows with position and diminishes with inertia. Expression (5.2) is based on the fact that the viscous force arising from the elongational terms in the momentum balance equation, or the velocity gradients in the x direction, is negligible, and is expected to

break down when $\frac{\partial u}{\partial x} \sim \frac{\partial u}{\partial z}$, or when $\delta \sim x - x_P$. For the

current problem, this happens when $x - x_P \sim Re^{-1}$. This relation will turn out to be in agreement with numerical predictions (see next). Recall that x_P is a function of the Reynolds number. In particular, $x_P(Re \rightarrow \infty) = 0$.

For a more accurate estimate of δ , consider first the variation of the velocity profiles with respect to height. Fig.8 displays typically the velocity profiles in the (x, z) plane inside the channel. Here $Re = 100$. The velocity profiles based on Tillett’s core solution (5.1) are also included (dashed lines). The figure indicates that the core solution tends to overestimate the velocity level near the wall because of the slip. The boundary layer height coincides with the level at

which the two velocity profiles begin to merge, as demonstrated in the figure.

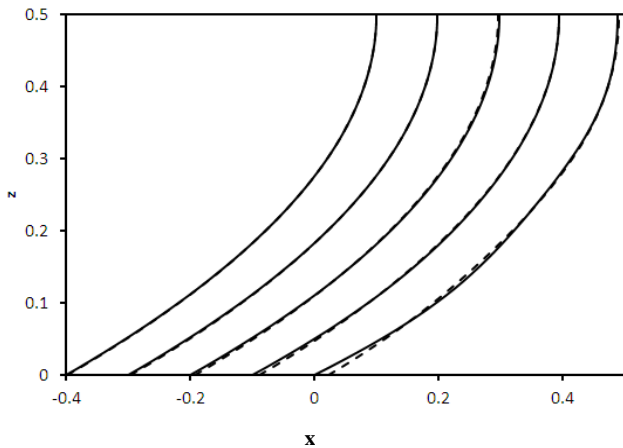


Fig. 8 Streamwise velocity profiles based on current formulation (solid lines) and Tillet's core solution (dashed lines) at different upstream positions for $Re = 100$

The influence of inertia on the boundary layer thickness is illustrated in Fig. 9.

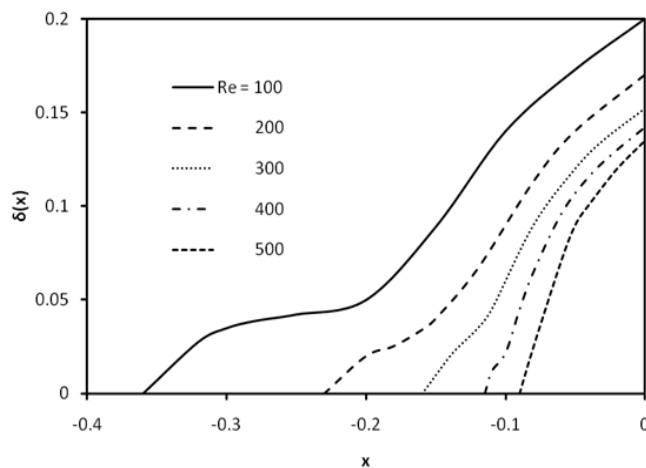


Fig. 9 Influence of inertia on the boundary layer thickness inside the channel

The figure also reflects the dependence of xP (edge of boundary layer) on Re , in agreement with the curve in Fig. 7 based on the wall shear stress criterion. The dependence of the boundary layer thickness on position and Reynolds number is in agreement with relation (5.2). However, as mentioned earlier, this behaviour is not sustained all the way to the channel exit. Instead, the boundary layer thickness follows a more rapid growth closer to the exit. The point of transition is also in agreement with the above estimate of $x - x_p \sim Re^{-1}$.

B. Boundary Layer Outside the Channel

The boundary layer thickness near the free surface $z = \zeta(x)$, or what Tillet termed as the inner layer, is now examined for $x > 0$. For the flow outside the channel, a suitable choice for the reference velocity u is the velocity at the free surface, which, from Tillet's equation (3.19), is given by $u(x > 0, z = \zeta) = 2.56 Re^{-1/3} x^{1/3} + O(Re^{-2/3})$. This yields in turn the following behaviour for the boundary layer thickness, namely

$$\delta(x > 0) \sim \left(\frac{x}{Re}\right)^{1/3} + O(Re^{-2/3}) \tag{5.3}$$

In comparison, the boundary layer thickness downstream from the channel exit for gravity driven free surface jet flow was shown by Wilson to grow like $\left(\frac{x}{Re}\right)^{1/4}$ [4]. Expressions (5.2) and (5.3) suggest that the boundary layer thickness inside the channel grows faster with distance and with the inverse of the Reynolds number than outside the channel. Also, the stress singularity at the exit tends to diffuse more rapidly downstream (over a shorter distance) for the more viscous fluid. In fact, the viscous relaxation length, x_∞ , outside the channel, can be estimated upon setting $\delta(x_\infty) = 0.5$, leading to $x_\infty \sim Re$ for both pressure and gravity driven jets. For $x > x_\infty$, the boundary layer contaminates the entire jet width. Since boundary layer theory neglects viscous forces arising from the elongational terms in the momentum balance equation, or the velocity gradients in the x direction, Tillet's inner layer approximation near the free surface is expected to break down when $\delta \sim x$. This happens when $x \sim Re^{-1/2}$ and $x \sim Re^{-1/3}$ for pressure and gravity driven jets, respectively.

The boundary layer thickness is determined more accurately upon comparing Tillet's composite flow to the flow in the outer region. The composite velocity is directly Tillet's expression (6.3), and the velocity in the outer layer is determined from Tillet's expression (4.1) for the stream function. Fig. 10 typically illustrates the velocity variation above the free surface of the jet outside the channel for the same Reynolds number as the profiles inside the channel in Fig. 8 ($Re = 100$).

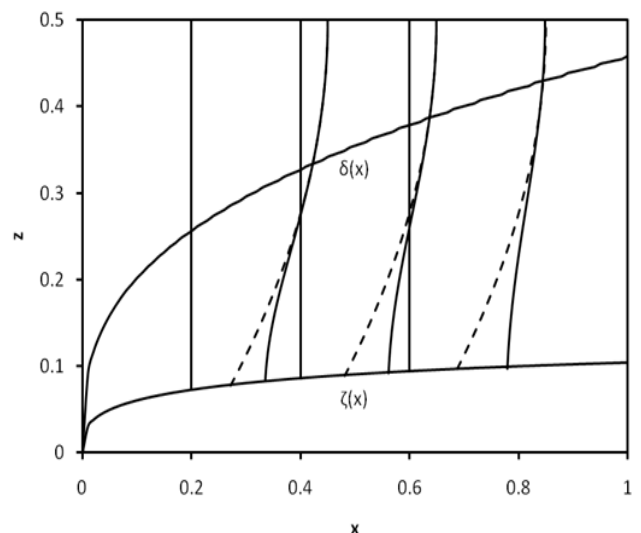


Fig. 10 Streamwise velocity profiles based on Tillet's solution at different downstream positions for $Re = 100$. The figure shows the composite (solid lines) and core (dashed lines) solutions. The boundary (inner) layer and free surface heights are also shown

The boundary layer height coincides with the level at which the composite and core velocity profiles begin to merge,

as demonstrated in the figure. The influence of inertia on the boundary layer thickness is illustrated in Fig. 11.

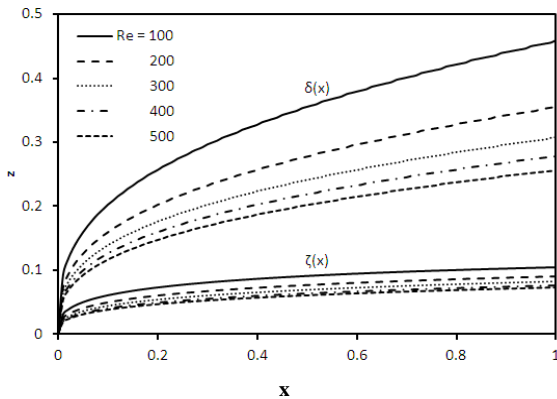


Fig. 11 Influence of inertia on the boundary layer thickness outside the channel. The free surface heights are also included. Profiles based on Tillett’s formulation

The free surface profiles, based on Tillett’s results [1], are also included for reference. The boundary layer thickness typically grows with position x . Outside the channel, the inner layer thickness continues to grow with position as the jet contracts, eventually prevailing over the entire film width. This is clearly illustrated for $Re = 100$ (see again Fig. 10).

VI. COMPARISON AGAINST COMPUTATIONAL METHODOLOGIES

The presence of the singularity does pose a serious hurdle when conventional numerical methods (using, for instance, finite difference or finite element discretization) are attempted. Although the singularity is not expected to be accurately captured by numerical methods, the issue to be addressed in this case is the extent to which the inaccuracy resulting from the presence of the singularity influences the rest of the computed flow field. The present problem offers an excellent opportunity to examine this issue. The flow of the jet emerging from the channel was determined using the computational software FLUENT. Comparison with the current high Reynolds number approach will be carried out for both inside and outside channel. The cases examined in this section all correspond to $Re = 1000$. This relatively high Reynolds number is chosen deliberately as it reflects a good accuracy of the current results inside the channel and Tillett’s results outside. Different mesh sizes are chosen in the Fluent calculations until reasonable convergence is achieved. Note, however, that too fine of a mesh size leads to excessive steepness near the singularity and not necessarily to more accurate results. Fig. 12 displays profiles of the centerline velocity based on the current formulation and numerical calculations.

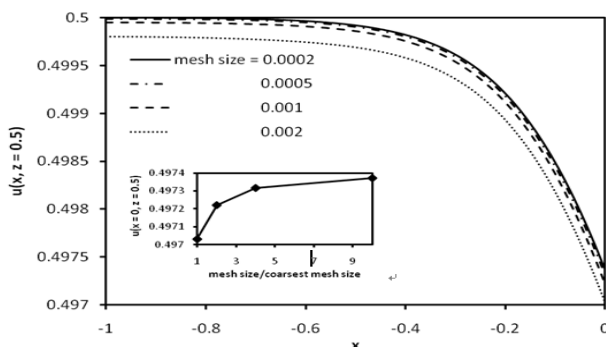


Fig. 12 Variation of centerline velocity with position for different mesh sizes based on the numerical result ($Re = 1000$)

The figure clearly shows good rate of convergence from the four mesh sizes used. There is also close agreement with the current results. This agreement and rapid rate of convergence is expected for this part of the flow given its remoteness from the singularity. Indeed, the comparison is not so favourable for the flow near the singularity. This is particularly obvious from the wall shear stress profiles depicted from Fig. 13.

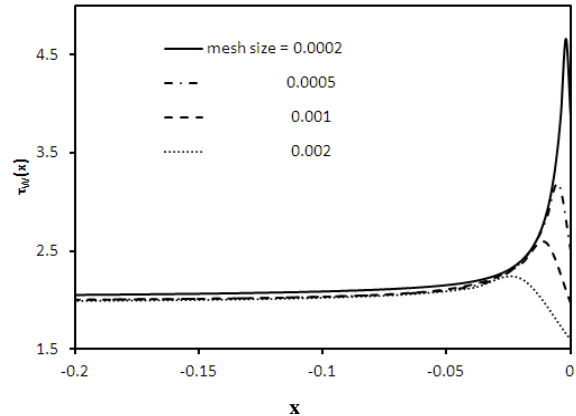


Fig. 13 Variation of skin friction with position for different mesh sizes based on the numerical result ($Re = 1000$)

While the current formulation suggests that the wall shear stress increases monotonically with x (see Fig. 6b), the computed wall shear stress displays a maximum near $x = 0$, which intensifies with mesh refinement. Upstream from the exit, all curves converge but not to the level predicted by the current analysis except much further upstream where fully developed conditions prevail. Indeed, the computed profiles indicate that fully developed conditions are reached at a point closer to the exit ($x = -0.05$) than the current formulation ($x = -0.6$ from Fig. 6b). Fig. 13 clearly reflects the unreliability of the computational approach in the neighbourhood of the exit near the wall. This inaccuracy is further illustrated when the free surface profiles are examined. Fig. 14 displays the jet profiles based on Fluent and Tillett’s formulation.

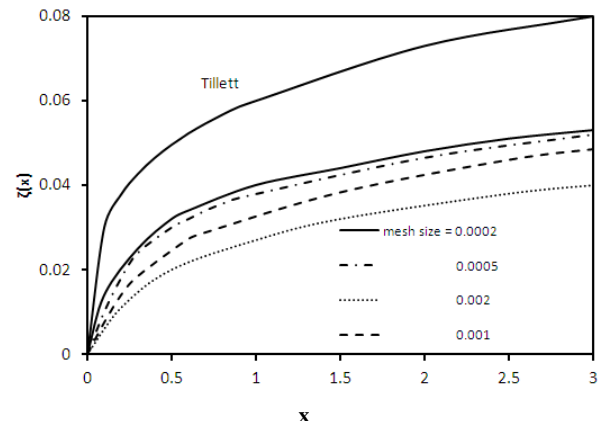


Fig. 14 Variation of free surface profile with position for different mesh sizes based on the numerical result and Tillett’s (1968) solution

In this case the discrepancy is significant. Convergence is once again attained with mesh refinement, but the error is on the order of 35% over the range of position shown in the figure. This discrepancy is mainly due to the singularity in height slope at $x = 0$, which cannot be captured by the computational approach. More importantly, the repercussion of this failure is felt everywhere downstream. In sum, while

the flow can be reasonably recovered using a computational approach, particularly inside the channel and far from the wall, a significant error is incurred for the flow outside the channel.

VII. DISCUSSION AND CONCLUSION

The aim of the current paper is to complement the work of Tillett^[1], and obtain a uniformly valid solution inside the channel, and examine closely the boundary layer structure near the wall upstream from the exit, and the extent to which this layer is influenced by the flow outside the channel. Inertia is assumed to remain relatively important, allowing the development of the flow field in terms of the inverse Reynolds number. The incoming flow is supposed to have the basic Poiseuille profile far upstream, and is modified when the fluid approaches and leaves the channel in the form of a free surface jet. When the fluid approaches the exit, the wall shear stress increases, which accompanied by the flattening of the velocity profile before the fluid detaches itself from the wall of the channel. This results in the drop of the wall shear stress at the channel exit, causing a boundary layer to form in a region near both the wall inside the channel and near the free surface outside. The boundary layer region inside the channel is predominantly of Poiseuille character, the departure being on the order of the inverse Reynolds number. However, a large velocity gradient is shown to develop at the wall, signaling some loss of viscous character as the velocity flattens. Outside the channel the almost parabolic velocity profile adjusts itself so as to satisfy the condition of zero traction at the free surface (assuming negligible surface tension effect). In the inviscid limit, the zero-traction condition does not hold, and the parabolic profile continues unchanged in the jet region. However, no uniqueness theorem exists for this inviscid problem, and it is conceivable that other solutions might exist. Nevertheless, and, similarly to Tillett^[1], it is assumed in this paper that Poiseuille flow is everywhere the proper inviscid limit. With this assumption, the flow in the core of the jet is, to leading order, not affected by the flow in the boundary layer region near the free surface or the wall. The boundary layer induces perturbations to the basic Poiseuille flow, when higher-order terms are included, both for the flow upstream and downstream from the channel exit.

In this study, the flow in the region upstream from the exit is assumed to comprise a Poiseuille component and a departure from it of $O(\text{Re}^{-1})$. The deviation flow field is then governed by an eigenvalue problem similar to entry flow^[7-9]. The eigenvalues are first estimated using Chandrasekhar function, which is then accurately determined along with the eigenfunctions by solving the two-point boundary-value problem. In particular, the flow field adjacent to the channel wall is examined where a boundary layer forms over moderate distance upstream from the channel exit.

The extent of this boundary layer diminishes with increasing Reynolds number. It is generally found that inertial effect is most significant close to the channel exit. Inspection of the flow at the centerline reveals that Poiseuille conditions for velocity and pressure are reached inside the channel at a distance about half width of the channel. Along the centerline, the pressure relaxes to zero level at a distance about one width of channel downstream from the channel exit whereas the streamwise velocity decreases with x (linearly for $x > 0$), suggesting the overall flattening of the velocity profile as a result of mass conservation.

REFERENCES

- [1] J. P. K. Tillett. On the laminar flow in a free jet of liquid at high Reynolds numbers. *J. Fluid Mech.* **32** (1968) 273.
- [2] Y. Miyake, E. Mukai and Y. Iemoto. On a two-dimensional laminar liquid jet. *Bull. Japan Soc. Mech. Eng.* **22**:72 (1979) 1382.
- [3] C. Philippe and P. Dumargue. Étude de l'établissement d'un jet liquide laminaire émergent d'une conduite cylindrique verticale semi-infinie et soumis à l'influence de la gravité. *J. Appl. Math. Phys. ZAMP* **42** (1991) 227.
- [4] D. E. Wilson. A similarity solution for axisymmetric viscous-gravity jet. *Phys. Fluids.* **29**(3) (1985) 632.
- [5] A. Saffari and R. E. Khayat. Flow of a viscoelastic jet with moderate inertia near exit. *J. Fluid Mech.* **639** (2008) 65.
- [6] I. J. Sobey. *Interactive boundary layer theory* (Oxford University Press, Oxford 2005).
- [7] F. T. Smith. Flow through constricted or dilated pipes and channels: Part I *Q. J. Mech. Appl. Math.* **29** (1976) 343.
- [8] F. T. Smith. Flow through constricted or dilated pipes and channels: Part II *Q. J. Mech. Appl. Math.* **29** (1976) 365.
- [9] F. T. Smith. The separating flow through a severely constricted symmetric tube *J. Fluid Mech.* **90** (1979) 725.
- [10] S. Wilson. Development of Poiseuille flow. *J. Fluid Mech.* **38** (1968) 497.
- [11] C. D. Eggleton, J. H. Ferziger and T. H. Pulliam. Moderate Reynolds number entry flow and boundary layer approximations for a viscoelastic fluid. *Phys. Fluids.* **6** (1994) 700.
- [12] J. R. Stocker and P. W. Duck. Stationary perturbations of Couette-Poiseuille flow: the flow development in long cavities and channels. *J. Fluid Mech.* **292** (1995) 153.
- [13] R. E. Khayat and S. L. Welke. Influence of inertia, gravity and substrate topography on the two-dimensional transient coating flow of a thin Newtonian fluid film. *Phys. Fluids* **13** (2001) 355.
- [14] S. Middleman. *Axisymmetric jet flow* (McGraw Hill, New York 2001).
- [15] G. J. Donnelly and C. B. Weinberger. Stability of isothermal fiber spinning of a Newtonian fluid. *Ind. Eng. Chem. Fund.* **14** (1975) 334.
- [16] R. E. Khayat, F. Cao and J. E. Puskas. Effect of inertia and gravity on the draw resonance in high-speed film casting of Newtonian fluids. *Int. J. Solids Structures* **42** (2005) 5734.
- [17] S. Chandrasekhar and W. H. Reid. On the expansion of functions which satisfy four boundary conditions. *Proc. Nat. Acad. Sci.* **43** (1957) 521.
- [18] M. Gottlieb and R. B. Bird. Exit effects in non-Newtonian liquids. An experimental study. *Ind. Eng. Chem. Fund.* **18** (1979) 357.